www.amlett.com, www.vbripress.com/aml, DOI: 10.5185/amlett.2015.5632 Published online by the VBRI press in 2015

Structural analysis by rietveld method and its correlation with optical propertis of nanocrystalline zinc oxide

Vikash Kumar[1], Swati Kumari[1], Pawan Kumar[2], Manoranjan Kar[2], Lawrence Kumar[1*]

[1]*Center for Nanotechnology, Central University of Jharkhand Ranchi, Ranchi 835205, India*
[2]*Department of Physics, Indian Institute of Technology Patna, Patna 800013, India*

[*]Corresponding author. Tel: +91-06531-292531; E-mail: lawrencecuj@gmail.com

Received: 09 September 2014, Revised: 30 October 2014 and Accepted: 15 November 2014

ABSTRACT

The correlation between structural and optical properties of nanocrystalline ZnO synthesized by the citrate precursor method has been investigated. The Rietveld refinement of X-ray diffraction pattern confirms the $P6_3mc$ space group and formation of single phase hexagonal wurtzite structure with presence of tensile strain at the lattice site. The presence of Raman active optical phonon mode at 436 cm^{-1} which is a significant character of ZnO with hexagonal wurtzite structure supports the XRD result. FE-SEM result shows that the size of the particle is about 20 nm with nearly spherical shapes. The optical band gap energy at room temperature has been calculated as 3.28 eV using the Tauc plot technique. The UV-Vis sub-gap absorption curve supports the presence of strain inside the crystal. The photoluminescence spectrum indicates the dominancy of the defect related deep level or trap state emissions over the near band edge UV emissions using an excitation wavelength of 320 nm. Copyright © 2015 VBRI press.

Keywords: X-ray diffraction; rietveld; wurtzite; Raman spectroscopy; photoluminescence.

Pawan Kumar is presently pursuing his Ph.D. at Dept. of Physics, Indian Institute of Technology Patna, India. He received his M.Sc. (Physics) degree from Patna University in 2011. His research interest includes Experimental Condensed Matter Physics.

Manoranjan Kar is Assistant Professor at Department. of Physics, Indian Institute of Technology Patna, India since 2008. He had completed his Ph.D. from IIT Guwahati in 2004. He has published more than 60 research articles in reputed journals. His present research interest includes Experimental Condensed Matter Physics.

Lawrence Kumar is Assistant Professor at Center for Nanotechnology, Central University of Jharkhand, Ranchi, India. He did M.Sc (Physics) from Patna University, India, M.Tech in Materials Science and Technology from IIT-BHU (Varanasi) and PhD from IIT Patna, India. He has 15 international publications to his credit. His research interest includes nanostructured magnetic and electronic materials.

Introduction

Research activities on the wide band gap oxide semiconductors such as TiO_2, CuO_2, SnO_2 and ZnO etc are under focus for the last few decades. These semiconductors have an electronic band gap greater than 1eV at room temperature. The devices based on these oxide semiconductors have an ability to operate at higher temperature as well as bring down the electronic transition in the range of visible light **[1]**. The energy band gap in these materials is of direct type which is defined as an occurrence of the minima of conduction band and maxima of valence band at the same k value where an electron can directly emit a photon. Among them, zinc oxide is a unique material that exhibits semiconducting, piezoelectric and pyroelectric multiple properties. ZnO is also referred as an II-VI compound semiconductor whose ionicity resides at the borderline between covalent and ionic semiconductor. ZnO is a direct wide band gap semiconductor. The band gap of ZnO is 3.44 eV at low temperatures and 3.37 eV at room temperature. Hence, it is colourless due to its large band gap. Its free-exciton binding energy is 60 meV. This large exciton binding energy indicates that efficient excitonic emission in ZnO can persist at room temperature as well as high temperature. It exhibits near-ultraviolet emission. ZnO crystal (particular in thin film form) exhibits second and third order non-linear optical behavior, which is

suitable for non-linear optical devices. The linear and non-linear optical properties of ZnO depend on the crystallinity of the samples **[2-5]**. The crystal structures shared by ZnO are wurtzite, zinc blende and rock salt. The thermodynamically stable phase of ZnO at ambient conditions is wurtzite. The zinc blende ZnO structure can be stabilized only by growth on cubic substrates, and the rock salt NaCl structure may be obtained at relatively high pressures. ZnO occurs naturally in the hexagonal wurtzite-type structure which belongs to crystallographic space group $P6_3mc$ **[6]**. The crystal structure of ZnO is considered as a non-centro symmetric structure and it give rise to spontaneous polarization. Its crystal structure can be described as a number of alternating planes composed of tetrahedral coordinated (bonded) O^{2-} and Zn^{2+} ions, stacked alternately along the c-axis (also known as polar axis). The stacking takes place along [0001] direction. The oppositely charged ions resulting in two polar surfaces {0001} with the positively charged (0001) surface being zinc terminated and negatively charged (0001) surface being terminated by oxygen resulting in a normal dipole moment and spontaneous polarization directed along the [0001] direction (c axis) of the crystal lattice **[7-11]**. It is a versatile functional material that has a diverse group of growth morphology such as nanocomb, nanoring, nanorod, nanowire, nanocages, nanobelts etc. making it richest family of nanostructures among all materials both in properties and structure **[12]**. Understanding the fundamental physical properties of these nanostructures is crucial to the rational design of functional devices which requires details study of its structural properties. The Rietveld method is a one of the powerful technique to extract detailed structural information of nanocrystalline materials.

Although Zn-O has very rich physical and chemical properties to be used in the technology, the ZnO-based devices have been limited to only sensing applications (e.g. gas sensor, humidity sensor etc.) till today. As there is lack of understanding and experimental evidences on the determination of chemical and/or crystallographic origin of visible bands due to intra gap states in the emission spectra, theoretical as well as experimental investigation are carried out to use ZnO-based materials in optoelectronics applications **[13]**. Hence, it is of the utmost importance that the correlation between crystal structure and optical properties of ZnO-based oxide semiconductors be fully understood for rational design of functional devices because of being promising materials for transparent oxide electronics and blue LED applications **[14]**. Hence, the detailed investigation on the correlation between structural and optical properties of nanocrystalline ZnO has been reported in this article.

Experimental

Materials

Nanocrystalline Zinc oxide (ZnO) compound has been synthesized by the citrate gel method. Zinc acetate $Zn(CH_3COO)_2.2H_2O$ and citric acid ($C_6H_8O_7.H_2O$) (all are of purity ≥ 99%, Merck Ltd., India) were used as starting materials. All the chemicals were of analytical grades.

Synthesis

The aqueous solution of zinc acetate and citric acid were obtained by dissolving it in deionized water. An aqueous solution of citric acid was mixed with the above zinc acetate solution. The mixed solution was kept on a hot plate with a continuous stirring at 90 °C. The citric acid plays two important roles: on one hand, it provides fuel for the reaction, as decomposition of citric acid in the solution liberates heat (exothermic process) which implies that the heat required for chemical reaction is provided by the reaction itself. The mixture solution became viscous during evaporation and finally formed a very viscous gel. This viscous gel was dried in a heating oven at 100 ^{0}C for 10 hours in order to remove excess water and finally it was heat treated in air atmosphere at 600 ^{0}C for 2 hour to get the resultant material.

Characterization

The crystalline phase of the sample have been examined by powder X-ray diffraction pattern using Cu-rotating anode based Rigaku TTRX-III X-ray diffractometer, Japan operating at 5 kW using the Cu-K_α radiation ($\lambda = 0.154$ nm) operating in the Bragg-Brentano geometry in 2θ range of 10^o-80^o. The surface morphology of the samples has been studied using FE-SEM (Hitachi S-4800, Japan). Raman spectrum of the present sample has been measured in the backscattering geometry using micro-Raman spectrometer (Seki Technotron Corp., Japan) with the 514.5 nm laser line as excitation source by STR 750 RAMAN spectrograph. A 100x microscope was used to focus the laser beam and collects the scattered light. The energy band gap of the sample has been determined using LAMBDA 35 UV-visible spectrophotometer (PerkinElmer, USA) in the range from 200 to 1100 nm. Photoluminescence spectrum was recorded using LS 55 Fluorescence Spectrometer (PerkinElmer, USA) with the excitation wavelength of 320 nm. All the above characterization has been carried out at room temperature.

Results and discussion

Powder X-ray diffraction analysis

The XRD pattern for the sample ZnO at room temperature has been shown in **Fig. 1**. The diffraction pattern consists of well resolved peaks which have been indexed to $P6_3mc$ space group in wurtzite symmetry. All the diffraction peaks are well matched with the JCPDS card no PDF 36-1451. The observed diffraction peaks corresponding to reflection planes (100), (002), (101), (102), (110), (103), (200), (112) and (201) provide a clear evidence for the formation of a single phase wurtzite structure for the ZnO system under study.

The XRD pattern has been analysed employing Rietveld technique with the help of the Fullprof Suite program using the $P6_3mc$ space group. The X-ray diffraction patterns along with Rietveld refined data has been shown in the **Fig. 2**. It could be seen that the profiles for observed and calculated ones are matching to each other and all the experimental peaks are allowed Bragg 2θ positions for $P6_3mc$ space group. The oxygen positions have been taken as free parameters during the refinement. The atomic

fractional positions for zinc have been fixed. Isothermal parameters and occupancies are fixed for both zinc and oxygen. Other parameters such as lattice constants, scale factors and shape parameters have been taken as free parameters during the fitting. The global parameters such as background and scale factors were refined in the first step of refinement. In the next step, the structural parameters such as lattice parameters, profile shape, width parameter, preferred orientation, asymmetry and atomic coordinates were refined in sequence. Background has been fitted with sixth order polynomial while the peak shapes have been described by pseudo-voigt profiles. The refined fractional atomic positions and isothermal parameters of the atoms obtained from Rietveld refinement are given in **Table 1**.

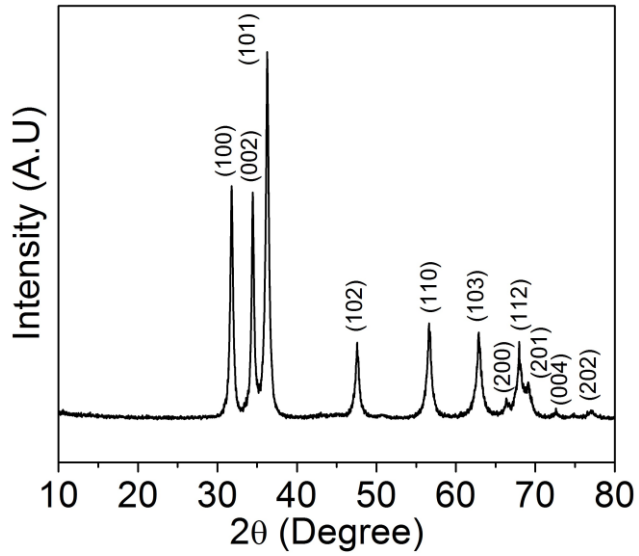

Fig. 1. XRD pattern of the sample ZnO.

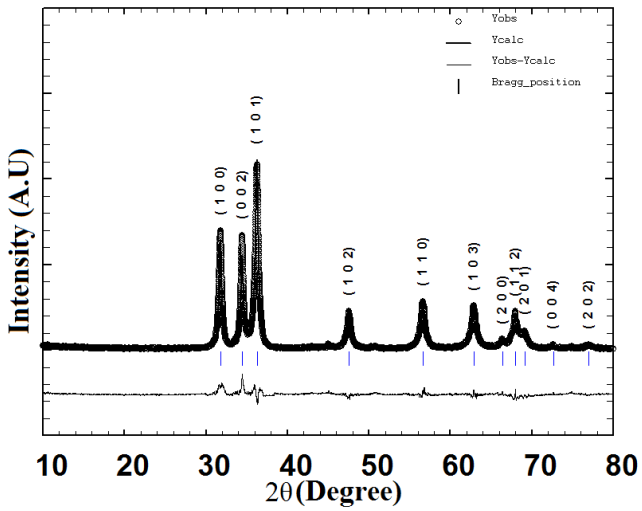

Fig. 2. Rietveld refined XRD pattern for the sample ZnO. The circles represent experimental points and the solid line represents Rietveld refined data. The bottom line shows the difference between the experimental and refined data. The marked 2θ positions are the allowed Bragg peaks.

The fitting quality of the experimental data have been assessed by computing the parameters such as the "goodness of fit" χ^2, and various *R*-factors such as R_p (profile factor), R_{wp} (weighted profile factor), R_{exp} (expected weighted profile factor), R_B (Bragg factor) and R_F (crystallographic factor) which are defined as follows **[15]**:

$$\text{Profile factor, } R_p = 100\frac{\sum_{i=1,n}|y_i - y_{c,i}|}{\sum_{i=1,n} y_i} \qquad (1)$$

where, 'y_i' is the observed point (experimental) and '$y_{c,i}$' is the calculated point and n represents the number of data points.

Table 1. Fractional atomic coordinates and isothermal parameter of different atoms obtained from the Rietveld analysis of XRD patterns for the sample ZnO.

Sample	**ZnO**			
Parameters→	***x***	**y**	**z**	B_{iso}
Atoms↓				
Zn	0.33333	0.66667	0.00000	0.06500
O	0.33333	0.66667	0.38224	0.07300

Weighted profile factor,

$$R_{wp} = 100\left[\frac{\sum_{i=1,n}\omega_i|y_i - y_{c,i}|^2}{\sum_{i=1,n}\omega_i y_i^2}\right]^{1/2} \qquad (2)$$

Where $\omega_i = \frac{1}{\sigma_i^2}$, σ_i^2 is the variance of observation y_i.

Expected weight factor,

$$R_{\exp} = 100\left[\frac{n-p}{\sum_{i=1,n}\omega_i y_i^2}\right]^{1/2} \qquad (3)$$

Here *(n – p)* is the number of degrees of freedom. '*n*' is the total number of experimental points and '*p*' is the number of refined parameters.

Reduced chi-square,

$$\chi^2 = \left[\frac{R_{wp}}{R_{\exp}}\right]^2 \qquad (4)$$

Bragg factor,

$$R_B = 100\frac{\sum_h|I_{obs,h} - I_{calc,h}|}{\sum_h I_{obs,h}} \qquad (5)$$

where, '*h*' is the vector which levels the Bragg reflections. The $I_{obs,\,h}$ is the observed integrated intensities and $I_{calc,\,h}$ is the calculated intensities.

Crystallographic R_F factor,

$$R_F = 100\frac{\sum_h \left|F_{obs,h} - F_{calc,h}\right|}{\sum_h F_{obs,h}} \quad (6)$$

The Reliability factors (*R* factors) R_p, R_{wp}, R_{Bragg}, R_F and χ^2 obtained from refinement are listed in the Table 2. One can see from the Table 2 that the values of *R* factors such as R_p and R_{wp} are found to be slightly large. Similar high values of *R* factors for nanocrystalline materials have been observed by others groups due to the lower value of diffraction peak to background ratio is low due to its nanocrystalline nature **[16-19]**. However, a low value of χ^2 (goodness of fit) has been observed which justifies the goodness of refinement. The Rietveld refinement yields lattice parameters and unit cell volume which are tabulated in **Table 2** along with the errors (in brackets). The observed lattice constant is in good agreement with those reported in literature **[20]**. The Zn-O bond length was calculated using refined atomic fractional coordinates and lattice parameters obtained from the Rietveld analysis. The Rietveld refinement study shows that oxygen occupies the specific position 1/3, 2/3 and *u* (**Table 1**) where the observed value of *u* is 0.38224. The parameter *u* represents the relative shift of the anionic sublattice with respect to cationic sublattice in *z* direction **[20]**. In an ideal wurtzite crystal structure of ZnO, the reported value of *c/a* and parameter *u* are 1.6333 and 3/8 (0.375) suggesting Zn-O bond lengths are identical along each axis direction. In the present study, the calculated values of *c/a* and *u* parameter are 1.6018 and 0.3822 respectively. The deviation in value of *c/a* and *u* parameter from the ideal structure suggests that the Zn-O bond length in the *c* axis direction is different in comparison with the other axis direction. The bond length in the *c* direction can be calculated by the relation uc. In other direction, it can be obtained by $\left[\frac{a^2}{3} + \left(\frac{1}{2} - u\right)^2 c^2\right]$ **[20]**. The calculated Zn-O bond distance along the *c* axis is 1.9877 whereas Zn-O bond distance perpendicular to the c axis is 1.9695. The observed values of Zn-O bond distance are consistent with the values reported in the literature **[20]**.

The crystallite size and lattice strain of the present sample have been extracted by analyzing the peak broadening of the XRD pattern using Williamson-Hall method. Peak broadening comes from several sources i.e. instrumental effect, finite crystallite size and strain effect within the crystal lattice. According to Williamson- Hall method individual contributions to the broadening of reflections can be expressed as **[21].**

$$\beta Cos\theta = \frac{k\lambda}{D} + 4\varepsilon Sin\theta \quad (7)$$

where, λ is the wavelength of the X-ray, θ is Bragg's diffraction angle, *D* is the crystallite size, β is Full width at Half Maximum (FWHM) of Intensity (a.u.) vs. 2θ profile and $4\varepsilon Sin\theta$ is the strain effect. The broadening β_{hkl} (FWHM) and 2θ (position of peak centre in degree) have been estimated by fitting the diffraction peak profile to Gaussian function. The crystal has been assumed to be isotropic in nature and strain is uniform in all crystallographic directions for Williamson equation (Eq. (7)). The Williamson Hall plot (βCosθ versus 4Sinθ) for the sample ZnO has been shown in **Fig. 3**. Strain and particle size have been estimated from the slope and y-intercept of the fitted line respectively. The estimated size of the particle and strain are 22 nm and 0.003 respectively. The W-H plot (**Fig. 3**) shows a positive slope which indicates the presence of tensile strain at the lattice site **[22]**.

Table 2. Reliability factors (R_p, R_{wp}, R_{Bragg}, R_F and χ^2), lattice constant, and crystallite size for the sample ZnO. Errors of the lattice parameters have been shown in bracket. For example, 3.3678 (94) means 3.3678±0.0094.

Parameters	Values
R_p (%)	10.1
R_{wp} (%)	13.1
R_{exp} (%)	8.33
R_B (%)	6.48
R_F (%)	4.17
χ^2	1.81
a=b (Å)	3.25094 (33)
c(Å)	5.20753(33)
Crystallite size (nm)	20
W-H plot	

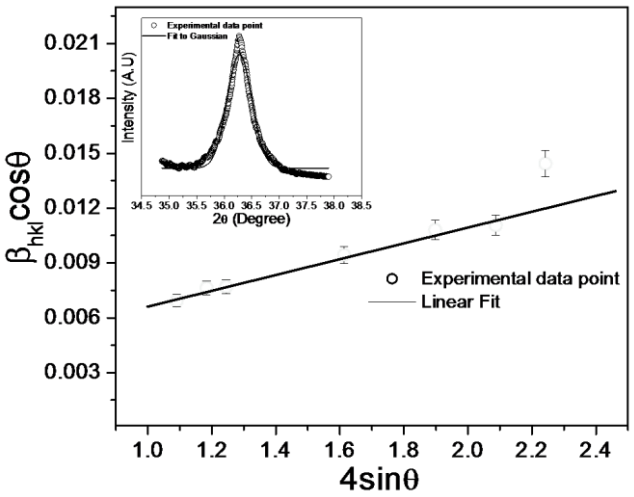

Fig. 3. Plot of β_{hkl} cos θ vs 4 sin θ. Inset shows fitting of Gaussian to highest intense peak (101).

In addition to particle size and lattice strain, one could also calculate the uniform stress inside the crystal by modifying the Williamson Hall equation (Eq. 7) using Hook's Law approximation. According to Hook's Law, there is linear proportional relation between the stress and strain for a small strain represented as $\sigma = Y\varepsilon$, where σ is the stress of the crystal and Y is the modulus of elasticity or Young modulus. Using the Hooke's law approximation to

Eq. (7), the modified form of Williamson equation is represented as-

$$\beta Cos\theta = \frac{k\lambda}{D} + \frac{4\sigma Sin\theta}{Y_{hkl}} \quad (8)$$

The Young's modulus for a hexagonal crystal is represented by the following relation **[23]**:

$$Y_{hkl} = \frac{\left[h^2 + \frac{(h+2k)^2}{3} + \left(\frac{al}{c}\right)^2\right]^2}{S_{11}\left(h^2 + \frac{(h+2k)^2}{3}\right)^2 + S_{33}\left(\frac{al}{c}\right)^4 + (2S_{13} + S_{44})\left(h^2 + \frac{(h+2k)^2}{3}\right)\left(\frac{al}{c}\right)^2}$$

---------- (9)

where S_{11}, S_{13}, S_{33}, S_{44} are the elastic compliances of ZnO having values 7.858 $\times 10^{-12}$, -2.206×10^{-12}, 6.940×10^{-12}, 23.57×10^{-12} m^2N^{-1} respectively **[24]**. Using Eq. (9) the calculated value of Young modulus Y for hexagonal zinc oxide nanoparticles is around ~126 GPa. The stress inside the crystal has been calculated from the plot drawn between $\beta_{hkl}Cos\theta$ on the Y-axis and $(4Sin\theta)/Y_{hkl}$ on the X- axis which is depicted in **Fig. 4**. The linear fitting to data yields the value of stress which is around 133 MPa. The origin of the strain and stress in the present sample may be ascribed to the presence of defects such as point defects concentrations (oxygen vacancies, zinc interstitials), dislocations etc **[1, 25]**.

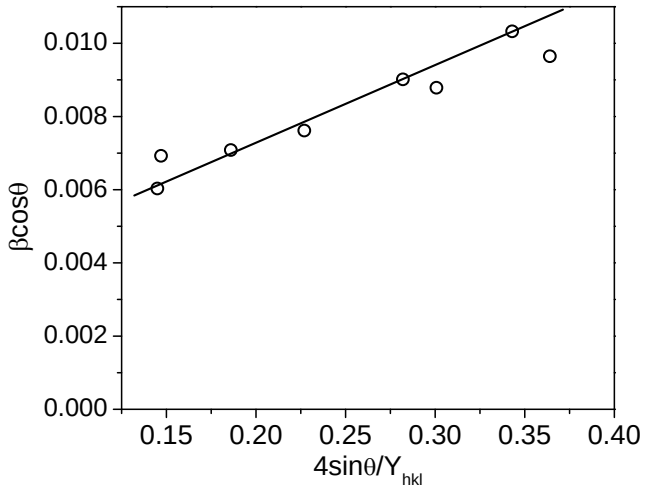

Fig. 4. Plot of β_{hkl} cosθ vs $4\sin\theta/Y_{hkl}$. Fit to data, the stress is extracted from the slope.

Particle size analysis

Morphology and estimation of the particle size have been carried out by FE-SEM. FE-SEM image of the sample ZnO is shown in **Fig. 5**. The image shows that most of the particles are uniform with nearly spherical shape with homogeneous distribution. The average size of the majority of the particles are in the range of ~ 20-22 nm as observed from the particle size distribution histogram (shown in **Fig. 6**), which is in good agreement with the particle size obtained by XRD analysis (discussed in previous section).

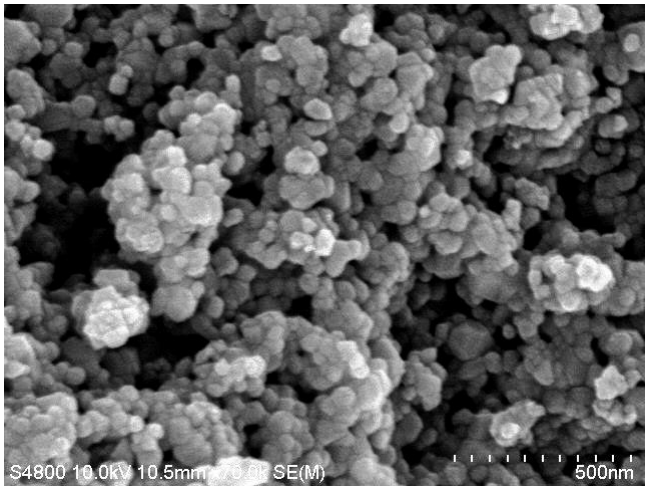

Fig. 5. FE-SEM image for the sample ZnO.

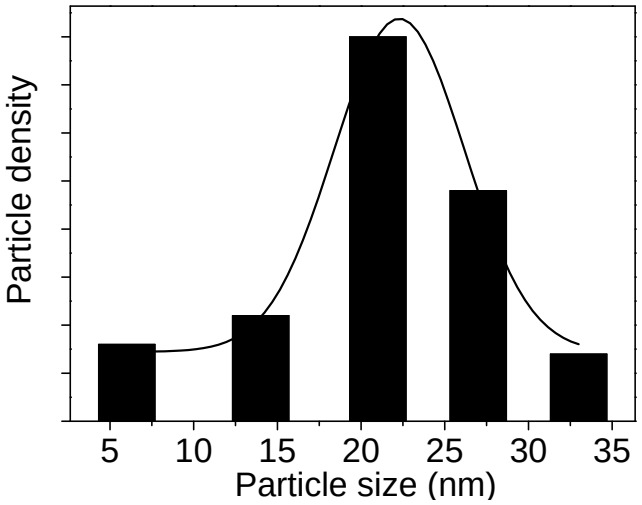

Fig. 6. Particles size distribution histogram with Gaussian fitting. The majority of the particles are in the range of 20- 22 nm.

Raman spectroscopy

The lattice dynamics in ZnO wurtzite structure compound (*6mm* point symmetry) has been examined by Raman spectroscopy. The wurtzite structure of ZnO consists of two formula units per unit cell (4 atoms per unit cell) leading to phonon dispersion relation consisting of 12 phonon branches (9 are optical and 3 are acoustic branches). The group theoretical analysis near the center of the Brillouin zone yields following phonon modes: $\Gamma = 2 \times (A_1 + B_1 + E_1 + E_2)$. Among these modes, the acoustic mode is given as $\Gamma_{acoustic} = A_1 + E_1$ and optical mode is represented as $\Gamma_{optical} = A_1 + 2B_1 + E_1 + 2E_2$.

The A_1 and E_1 branches are both Raman- and infrared-active, the E_2 branches are Raman-active only, while the B_1 branches are both Raman and infrared inactive according to the selection rules for phonon resonance modes. The phonons with A_1 and E_1 modes (symmetry) are polar which splits into transverse optical (represented as A_{1T} and E_{1T}) and longitudinal optical (represented as A_{1L} and E_{1L}) components with different frequencies. It is due to the long range electrostatic forces as well as crystal field associated with the phonons. The phonon vibration with A_1 symmetry

is polarized parallel to the C-axis whereas with E_1 symmetry, it is polarized perpendicular to the C-axis. The phonon with E_2 mode is non-polar consisting of low and high frequency phonons (represented as E_{2L} and E_{2H}) **[26-30]**. **Fig. 7** (**a**) shows the Raman spectrum of ZnO nanoparticles in the range of 200 - 2000 cm^{-1}. The spectrum has been fitted and it is deconvoluted into individual Lorentzian component in order to determine the peak position. The spectrum has been deconvoluted in the range of 270-600 cm^{-1} and 1000-1650 cm^{-1} which is depicted in **Fig. 7 (b)** and **(c)** with Lorentzian fitting. The Raman spectrum shows a strong sharp peak at 436 cm^{-1}. It is the significant character of the ZnO with hexagonal wurtzite structure. It corresponds to the vibration mode E_{2H} associated with the vibration of oxygen atom known as Raman-active optical phonon mode which is a strongest mode in the system of wurtzite structure **[30, 31]**. Moreover, the appearance of sharp peak at 436 cm^{-1} reflects the presence of induced stress in ZnO wurtzite crystal structure which is well supported by X-ray analysis (discussed in previous section) **[32]**. The appearance of peak at 325 cm^{-1} is assigned as $E_{2\ (high)}$-$E_{2\ (low)}$ mode. It is second order Raman process which arises due to zone boundary phonons of the hexagonal ZnO **[33]**. The peak at 381 cm^{-1} is attributed to A_1 transverse mode. It arises due to the anisotropy character of the force constant **[34]**. The peak at ~580 cm^{-1} could be ascribed to the longitudinal E_1 (LO) modes. It is due to the presence of Zn interstitials ($Zn_i^{\bullet\bullet}$) and oxygen vacancies ($V_O^{\bullet\bullet}$) which are usually caused by surface defects **[35]**. The presence of oxygen vacancies and other vacancies have also been well supported by Photoluminescence spectrum (discussed in next section). The Raman peak located at 674 cm^{-1} is an intrinsic mode of ZnO which may result from the two phonon process assigned as A_{1L}+E_{2L} **[36]**. The peaks obtained at ~1120, 1154, 1281, 1314, 1369, 1416, 1489, 1576 cm^{-1} are due to multiphonon modes and are matched with the reported values **[29]**.

UV analysis

Fig. 8 shows the absorbance spectrum for ZnO sample. It shows a sharp absorbance edge in the UV range. The absorption spectrum shows a very little absorption in the visible region which is the characteristic of ZnO sample. The optical band gap energy for the direct gap semiconductor in the parabolic band structure can be calculated from the Tauc plot using the following well known equation 10 **[37];**

$$\alpha = \frac{A(h\nu - E_g)^{\frac{1}{2}}}{h\nu} \qquad (10)$$

The "α" is absorption coefficient, "*A*" is a band edge sharpness constant, "E_g" is the band gap and hυ is the incident photon energy in Eq. 10. The band gap of ZnO sample is calculated by plotting $(\alpha h\upsilon)^2$ versus incident photon energy and linearly regressing the linear portion of the $(\alpha h\upsilon)^2$ to zero. The point where the line meets the energy axis represents the band gap energy **[37]**. The value of energy band gap is found to be 3.28 eV. The observed value of energy gap is slightly smaller than that of bulk ZnO sample which is reported to be 3.37 eV. It might be due to introduction of various defects such as vacancies etc. during the synthesis **[38]**.

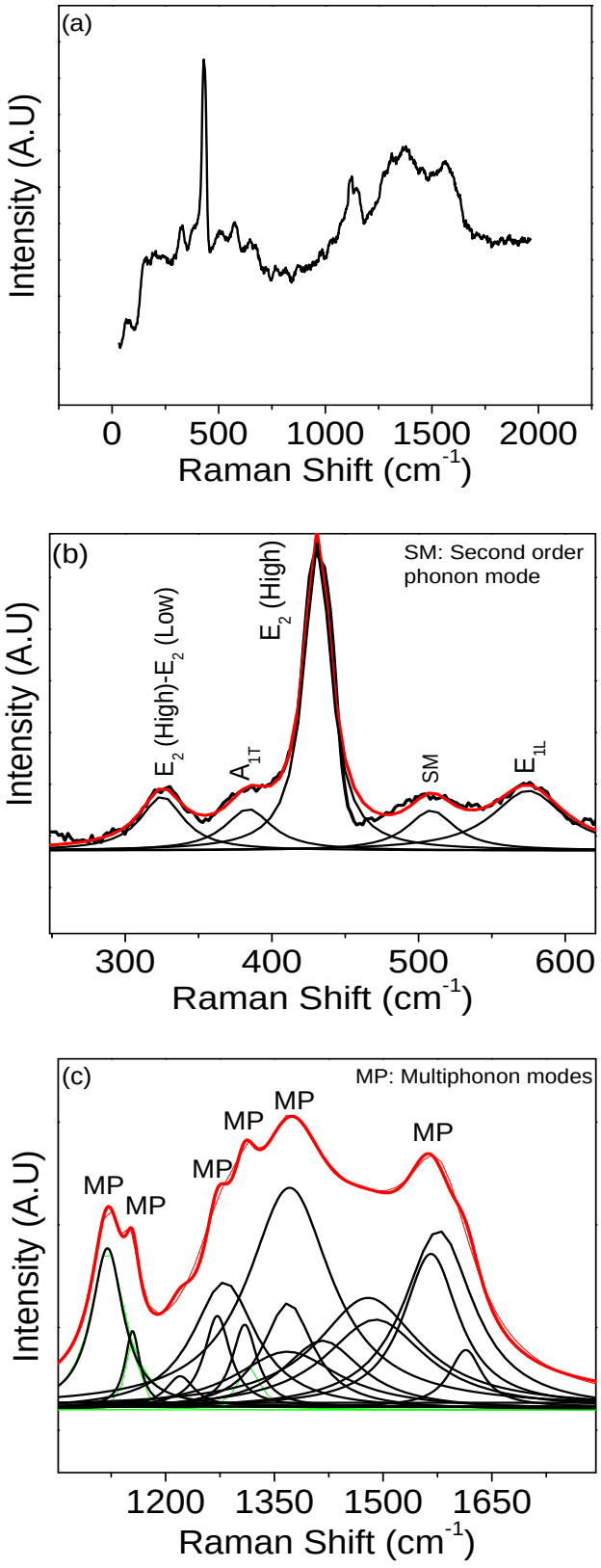

Fig . 7. (a) Raman spectra of the sample ZnO, (**b**) Lorentzian fitting within the range 270- 600 cm^{-1} and (**c**) Lorentzian fitting within the range 1000-1700 cm^{-1}.

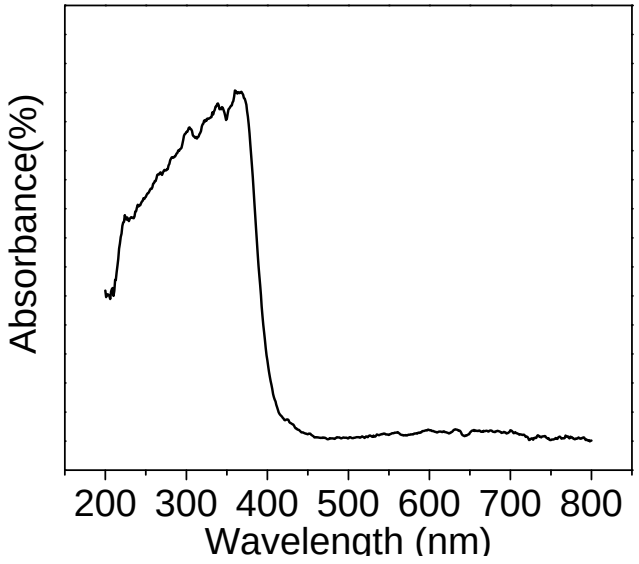

Fig. 8. UV-vis spectrum of ZnO.

One can extract the information about the strain inside the crystal by analyzing the UV-vis sub-gap-absorption curve **[25]**. **Fig. 9** shows a sub-gap-absorption curve which is a plot between Log absorption coefficients and incident photon energy. Sub-gap absorption is a fundamental process which measures the density of states as well as energy positions of all the states in the band gap. The sub-gap absorption curve as shown in **Fig. 9** shows non-zero slope which reflects the presence of strain inside the crystal and it supports the XRD analysis **[25]**. As discussed in the previous section, the origin of strain may be ascribed to presence of lattice defects such as dislocations, point defects etc. The presence of lattice defects induces strain inside the crystal give rise to localized density of states (DOS) in the band gap **[25]**.

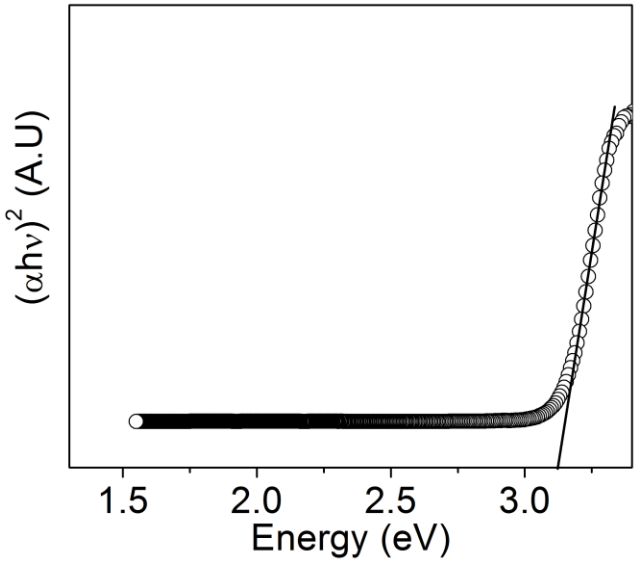

Fig. 9. Estimation of band gap using plot of $(\alpha h\nu)^2$ versus photon energy.

In view of the above, a correlation between the density of states (DOS) in the band gap and strain is expected as both density of states and strain has a common origin (lattice defects). Also, density of states (DOS) could be quantitatively estimated from the sub-gap absorption measurement. Further detail analysis is required to correlate the DOS in the band gap and estimated strain which is beyond the scope of the present study. The information about Urbach energy could be extracted from the plot of log (α) versus incident photon energy as shown in **Fig. 10** which corresponds to the width of the band tail. The absorption coefficient near the band edge shows an exponential dependence on photon energy which is represented as Eq. 11 **[37]**;

$$\alpha = \alpha_0 \exp\left[\left(h\nu - E_i\right)\Big/ E_u\right] \qquad (11)$$

The *"E_u"* is known as Urbach energy, E_i and α_o are constant in Eq. 11. The Urbach energy has been calculated from the reciprocal gradient of the linear portion of curve (shown in **Fig. 3**). The calculated value is 145 meV which is consistent with the values reported in the literature **[37]**.

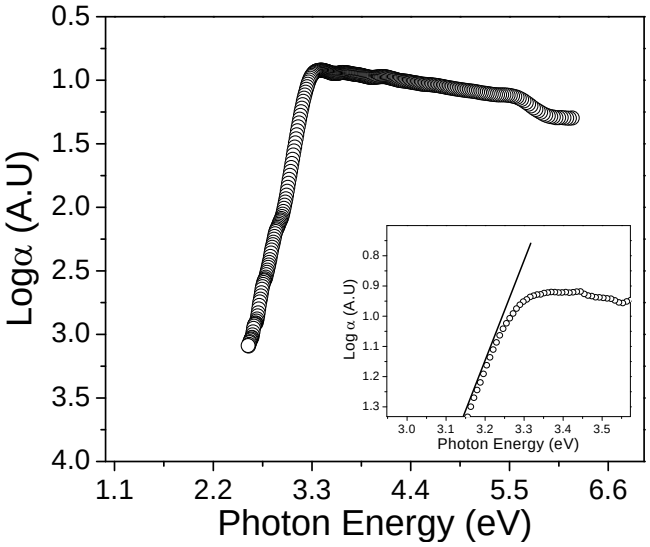

Fig. 10. Log absorption coefficient in the sub-band-gap-region plotted as a function of photon energy. Inset shows non-zero slope of the sub-gap absorption curve.

Photoluminescence study

Fig. 11 shows a photoluminescence spectrum for ZnO sample recorded at room temperature. The emission spectra were recorded using 320 nm excitation. In the present study, the PL spectrum shows that all the emission peaks have been appeared in visible region. It indicates that PL emission from the sample is dominated by the defect related deep level or trap state emission over the near band edge UV emission. The defects present in the sample are oxygen vacancies (V_O), oxygen intersites (O_i), zinc interstitials (Zn_i), zinc vacancies (V_{Zn}) and surface dangling bonds which are responsible for emission peaks in the visible range **[39]**. The positions of these zinc intersites, zinc vacancies, oxygen vacancies and oxygen intersites band have been predicted theoretically. The positions of the zinc interstitials and zinc vacancies are located at 0.22eV and 3.06eV below the conduction band respectively. Similarly oxygen vacancies and oxygen intersites are located at 0.9eV above the valence band and 2.28eV below the

conduction band respectively **[40]**. The spectrum shows emission peaks at 431 nm, 486 nm and 529 nm respectively.

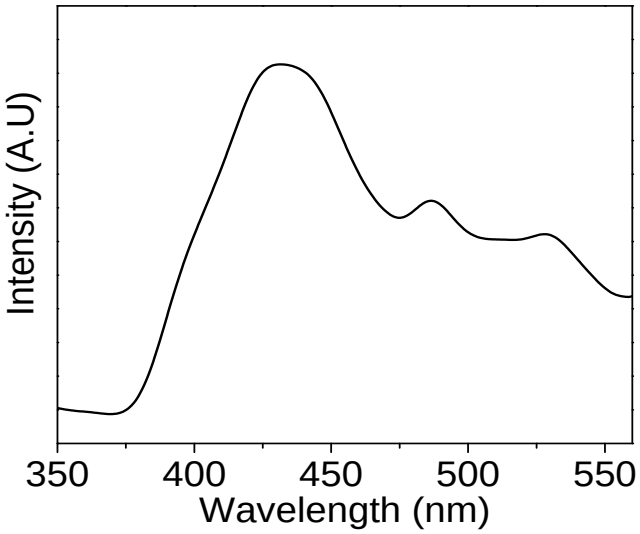

Fig. 11. Room temperature PL spectrum for ZnO sample.

The peak at 431 nm (2.87 eV) corresponds to the recombination between electron at zinc interstitials and hole in the valence band. The excited electron to the conduction band will relax to the zinc interstitial band through a non-radiative transition and then transition to the valence band yields emission in the violet region centered at 2.87 eV **[41]**. The emission peak at 486 nm (2.54 eV) corresponds to blue region **[37]** which is explained as follow: theoretically the energy interval from the zinc interstitial to zinc vacancies is approximately 2.84 eV. The emission peak at 486 nm corresponds to 2.54 eV which is in close agreement with the above theoretical value. This suggests that electrons have made transition from the conduction band to the zinc interstitials through a non-radiative process and then transition to the zinc vacancy enabling emission band in the blue region centered at 2.87 eV. The peak centered at 529 nm is refereed as green emission peak which is attributed to singly ionized oxygen vacancy (V_O) **[37, 42]**. It is believed that this green emission is due to transition of electrons from zinc interstitial (Zn_i) to oxygen vacancy (V_o) defect levels which can be explained as follow: The position of the Vo level is located approximately at 2.28 eV below the conduction band, and the position of the Zn_i level is theoretically located at 0.22 eV below the conduction band. Therefore, it is expected that the band transition from the Zn_i to the V_o level is approximately 2.06 eV. This agrees well with the observed green emission peak centered at 2.23 eV. However, the exact mechanism for these defect based emission located in the visible region is not fully understood yet.

Conclusion

In summary, single phase ZnO nanoparticles in wurtzite structure were successfully synthesized by the citrate precursor method and the particle size estimated by FE-SEM is in close agreement with the size obtained by XRD analysis using Rietveld analyis. The lattice strain in the sample ZnO have been estimated from the Williamson Hall plot (βCosθ versus 4Sinθ) and which is consistent with the observation from UV-Vis sub-gap absorption curve. The strongest peak located at 436 cm^{-1} in Raman spectrum confirms the wurtzite structure of the sample. The optical band gap energy of 3.28 eV have been estimated using the Tauc plot technique. The emission peak in PL spectrum is observed in the visible region which is due to presence of various point defects in ZnO lattice. The present study is interesting from the viewpoint of understanding the correlation between the structural and optical properties and to design the nanocrystalline ZnO with different surface to volume ratio and lattice strain which are the key parameters for modifying its properties. Hence, it may serve as a valuable reference for further experimental and theoretical studies in ZnO-based semiconductors.

Reference

1. Kumar, P.; Singh, J.; Parashar, V.; Singh, K.; Tiwari, R.S.; Srivastava, O. N.; Ramam, K.; Pandey, A. C.; *Cryst. Engg. Comm.*, **2012**, *14*, 1653. **DOI:** 10.1039/clce06127e
2. Mang, A.; Reimann, K.; Rubenacke, St.; *Soild. State. Commun*. **1995**, *94*, 251. **DOI:** 10.1016/0038-1098(95)00054-2
3. Madelung, O. Semiconductors-Basic Data; Springer: Berlin, **1996**. **DOI:** 10.1007/978-3-642-97675-9
4. Bagnall, D. M; Chen, Y. F; Zhu, Z; Yao, T; Koyama, S; Shen, M. Y; Goto, T.; *Appl. Phys. Lett.*, **1997**, *70*, 2230. **DOI:** 10.1063/1.118824
5. Corsa, A. D.; Posternak, M.; Resta, R.; Balderschi, A.; *Phys. Rev. B.*, **1994**, *50*, 10715. **DOI:** 10.1103/PhysRevB.50.10715
6. Jaffe, J. E.; Hess, A. C.; *Phys. Rev. B.*, **1993**, *48*, 7903. **DOI:** 10.1103/PhysRevB.48.7903
7. Wang, Z. L.; Kong, X. Y.; Ding, Y.; Gao, P.; Hughes, W. L.; Yang, R.; Zhang, Y.; *Adv. Funct. Mater*, **2004**, *14*, 943. **DOI:** 10.1002/adfm.200400180
8. Kong, X. Y.; Wang, Z. L.; *Nano. Lett*, **2003**, *3*, 1625. **DOI:** 10.1021/nl034463p
9. Kong, X. Y.; Ding, Y.; Yang, R.; Wang, Z. L.; *Science*, **2004**, *303*, 1348. **DOI:** 10.1126/science.1092356
10. Kong, X. Y.; Wang, Z. L.; *Appl. Phys. Lett*, **2004**, *84*, 975. **DOI:** 10.1063/1.1646453
11. Ludi, B.; Niederberger, M.; *Dalton. Trans*., **2013**, *42*, 12554. **DOI:** 10.1039/c3dt50610j
12. Rodriguez, J. A.; Garcia, M. F.; Synthesis, Properties and Applications of Oxide nanomaterials; Wiley & Sons: New Jersey **2007**. **DOI:** 10.1002/0470108975
13. Fabbri, F.; Villani, M.; Catellani, A.; Calzolari, A.; Cicero, G.; Calestani, D.; Calestani, G.; Zappettini, A.; Dierre, B.; Sekiguchi, T.; Salviati, G.; *Sci. Rep*. **2014,** *4*, 5158. **DOI:** 10.1038/srep05158
14. Nahm, H.-H.; Park, C.H.; Kim, Y.-S.; *Sci. Rep*. **2014**, *4*, 4124. **DOI:** 10.1038/srep04124
15. https://www.ill.eu/sites/fullprof/index.html
16. Chen, L.; Mashimo, T.; Omurzak, E.; Okudera, H.; Iwamoto, C.; Yoshiasa, A.; *J. Phys. Chem. C.*, **2011**, *115*, 9370. **DOI:** 10.1021/jp111367k
17. Im, J.-H.; Chung, J.; Kim, S.-J.; Pak, N.-G.; *Nanoscale. Res. Lett.*, **2012**, *7*, 353. **DOI:** 10.1186/1556-276X-7-353
18. Du, Y.; Fang, J.; Zhang, M.; Hong, J.; Yin, Z.; Zhang, Q.; *Mat. Lett.*, **2002**, *57*, 802. **DOI:** 10.1016/S0167-577X(02)00876-5
19. Bhagwat, M.; Ramaswamy, A. V.; Tyagi, A. K.; Ramaswamy, V. *Mat. Res. Bull*. **2003**, *38*, 1713. **DOI:** 10.1016/S0025-5408(03)00201-0

20. Brehm, J. U.; Winterer, M.; Hahm, H.; *J. Appl. Phys.*, **2006**, *100*, 064311.
DOI: 10.1063/1.2349430
21. Suryanarayana, C.; Nortan, M. G.; X-ray Diffraction: A practical Approach; Plenum Publishing Corporation: New York, **1998**.
DOI: 10.1007/978-1-4899-0148-4
22. Ahlawat, A; Sathe, V. G; Reddy, V. R; Gupta, A.; *J. Magn. Magn. Mater*. **2011**, *323*, 2049.
DOI: 10.1016/j.jmmm.2011.03.017
23. Zhang, J; Zhang, Y; Xu, K. W; Ji, V.; *Solid. State. Commun.* **2006**, *139*, 87.
DOI: 10.1016/j.ssc.2006.05.026
24. Nye, J. F.; Physical Properties of Crystals:Their Representation by Tensors and Matrices; Oxford: New York, **1985**.
25. Sinha, A. K.; Gupta, R. K.; Deb, S. K.; *Appl. Phys. A.*, **2012**, *108*, 607.
DOI: 10.1007/s00339-012-6938-y
26. Guo, S; Du, Z; Dai, S.; *Phys. Stat. Sol (b)* **2009,** *246*, 2329.
DOI: 10.1002/pssb.200945192
27. Ozgur, U.; Alivov, Y.I.; Liu, C; Teke, A.; Reshchikov, M.A.; Dogan, S.; Avrutin, V.; Cho S-J; Morkoc, H.; *J. Appl. Phys.*, **2005**, *98*, 041301.
DOI: 10.1063/1.1992666
28. Rajalakshmi, M.; Arora, A. K.; Bendre, B. S.; Mahamuni, S.; *J. Appl. Phys*. **2000**, *87*, 2445.
DOI: 10.1063/1.372199
29. Cusco, R.; Alarcon-Llado, E.; Ibanez, J.; Artus, L.; Jimenez, J.; Wang, B.; Callahan, M. J.; *Phys. Rev. B.*, **2007**, *75*, 165202.
DOI: 10.1103/PhysRevB.75.165202
30. Giri, P. K.; Bhattacharyya, S; Singh, D. K; Kesavamoorthy, R; Panigrahi, B. K; Nair, K. G. M.; *J. Appl. Phys*., **2007**, *102*, 093515.
DOI: 10.1063/1.2804012
31. Liu, B.; Zeng, H. C.; *J. Am. Chem. Soc.*, **2003**, *125*, 4430.
DOI: 10.1021/ja0299452
32. Ben Yahia, S; Znaidi, L; Kanaev, A; Petitet, J. P.; *Spectrochim. Acta. A.*, **2008**, *71*, 1234.
DOI: 10.1016/j.saa.2008.03.032
33. Alim, K. A; Fonoberov, V. A.; Shamsa, M.; Balandin, A. A.; *J. Appl. Phys.*, **2005**, *97*, 124313.
DOI: 10.1063/1.1944222
34. Lehr, D.; Luka, M.; Wagner, M. R.; Bügler, M; Hoffmann, A; Polarz, S; *Chem. Mater.*, **2012**, *24*, 1771.
DOI: 10.1021/cm300239q
35. Umar, A.; Kim, S. H.; Lee, Y. S.; Nahm, K. S.; Hahn, Y. B.; *J. Cryst. Growth*, **2005**, *282*, 131.
DOI: 10.1016/j.jcrysgro.2005.04.095
36. Serrano, J.; Romero, A. H.; Manjon, F. J.; Lauck, R.; Cardona, M; Rubio, A.; *Phys. Rev. B.*, **2004**, *69*, 094306-1.
DOI: 10.1103/PhysRevB.69.094306
37. Vasile, O-R; Andronescu, E; Ghitulica, C; Vasile, B, S; Opera, O; Vasile, E; Trusca, R.; *J. Nanopart. Res.*, **2012**, *14*, 1269.
DOI: 10.1007/s11051-012-1269-7
38. Wang, X. C.; Chen, X. M.; Yang, B. H. *J. Alloys. Compd.* **2009**, *488*, 232.
DOI: 10.1016/j.jallcom.2009.08.089
39. Pandiyarajan, T.; Baesso, M. L.; Karthikeyan, B.; *Eur. Phys. J. D.* **2014**, *68*, 28.
DOI: 10.1140/epjd/e2013-40363-3
40. Ahn, C. H.; Kim, Y. Y.; Kim, D. C.; Mohanta, S. K.; Choa, H. K.; *J. Appl. Phys.*, **2009**, *105*, 013502.
DOI: 10.1063/1.3054175
41. Zeng, H.; Duan, G.; Li, Y.; Yang, S.; Xu, X.; Cai, W.; *Adv. Funct. Mater*., **2010**, *20*, 561.
DOI: 10.1002/adfm.200901884
42. Samanta, P. K; Bandyopadhyay, A. K.; *Appl. Nanosci.* **2012**, *2*, 111.
DOI: 10.1007/s13204-011-0038-8